

# Paleoceanography and Paleoclimatology\*

## RESEARCH ARTICLE

10.1029/2021PA004357

## Warmer Pliocene Upwelling Site SST Leads to Wetter Subtropical Coastal Areas: A Positive Feedback on SST

Minmin Fu<sup>1</sup> , Mark A. Cane<sup>2</sup> , Peter Molnar<sup>3,4</sup> , and Eli Tziperman<sup>1,5</sup> 

<sup>1</sup>Department of Earth and Planetary Sciences, Harvard University, Cambridge, MA, USA, <sup>2</sup>Lamont-Doherty Earth Observatory, Columbia University, Palisades, NY, USA, <sup>3</sup>Department of Geological Sciences, University of Colorado Boulder, Boulder, CO, USA, <sup>4</sup>Cooperative Institute for Research in Environmental Sciences, University of Colorado Boulder, Boulder, CO, USA, <sup>5</sup>School of Engineering and Applied Sciences, Harvard University, Cambridge, MA, USA

### Key Points:

- Warm Pliocene sea surface temperatures (SSTs) at midlatitude coastal upwelling sites are a common feature of proxy reconstructions
- Prescribing higher SSTs along the California coast in an atmospheric model increases rainfall over western North America
- Precipitation differences are caused by increased mean convergence during the boreal summer and enhanced eddy fluxes in the winter

### Supporting Information:

Supporting Information may be found in the online version of this article.

### Correspondence to:

M. Fu,  
mjfu@g.harvard.edu

### Citation:

Fu, M., Cane, M. A., Molnar, P., & Tziperman, E. (2022). Warmer Pliocene upwelling site SST leads to wetter subtropical coastal areas: A positive feedback on SST. *Paleoceanography and Paleoclimatology*, 37, e2021PA004357. <https://doi.org/10.1029/2021PA004357>

Received 30 AUG 2021

Accepted 29 DEC 2021

**Abstract** The early- to mid-Pliocene (5.3–3 Ma), characterized by warmer temperatures and similar CO<sub>2</sub> concentrations to present day, is considered a useful analog for future warming scenarios. Geological evidence suggests that during the Pliocene, many modern-day desert regions received higher levels of rainfall and supported large perennial lakes and wetter vegetation types. These wetter conditions have been difficult to reconcile with model predictions of 21st century drying over most subtropical land regions. Using an atmospheric General Circulation Model, we show that underestimates of Pliocene rainfall over certain areas in models may be related to insufficient sea surface temperature (SST) warmth simulated over relatively local eastern boundary current regions. When SSTs off the coast of California are raised to more closely match some proxy reconstructions, rainfall increases over much of adjacent western North America. Over the southwestern USA, this increased rainfall is mainly due to a convergent monsoonal circulation that develops over late boreal summer. A smaller wintertime increase in precipitation also occurs due to differences in rainfall associated with midlatitude cyclones. Wetter land conditions are expected to weaken upwelling-favorable coastal winds, so that increased rainfall caused by coastal SST warming suggests a positive feedback that could help sustain wet, Pliocene-like conditions.

## 1. Introduction

The early to middle Pliocene (5.3–3 Ma) was the most recent epoch of prolonged global warmth relative to modern day. Proxy records point to several notable differences between Pliocene and modern-day climates. The Pliocene was characterized by strongly polar-amplified warming (Dowsett et al., 1994; Thompson & Fleming, 1996), with slightly smaller Antarctic ice sheets and minimal Northern Hemisphere ice coverage (Ravelo et al., 2004). The mean east-west sea surface temperature (SST) gradient in the tropical equatorial Pacific may have been weaker (Chaisson & Ravelo, 2000; Dekens et al., 2008; Dowsett & Robinson, 2009; Wycech et al., 2020) and some studies suggest it was similar to that during modern El Niño events (K. T. Lawrence et al., 2006; Molnar & Cane, 2002, 2007; Ravelo et al., 2006; Wara et al., 2005). The character of the east-west equatorial SST gradient, however, continues to be debated (O'Brien et al., 2014; Tierney et al., 2019; Zhang et al., 2014).

More relevant to the specific goals of this work, some proxy reconstructions indicate that during the early- to mid-Pliocene, SSTs near midlatitude coastal upwelling zones, such as along the California coast, may have been as much as 9°C warmer than modern day (Brierley et al., 2009; Dekens et al., 2007; LaRiviere et al., 2012). This indicates that coastal upwelling may have functioned differently during the Pliocene. Coastal upwelling in the modern climate is driven by upwelling-favorable surface winds, which are geostrophically balanced by the contrast between the subtropical highs (regions of high surface pressure over oceans at around 20°S–40°S and 20°N–40°N), and the lower surface pressures over the warm, dry, western continental regions. This leads to alongshore wind stress parallel to shore, which causes offshore Ekman transport and cold upwelling from below. This upwelling forms a strip of cold water along the eastern side of major ocean basins, for instance, within the California, Canary, Humboldt, and Benguela upwelling systems. Although coastal upwelling at high rates occurs within tens of kilometers of the shore, the cold SST signal extends hundreds of kilometers offshore, with a decay scale set by the balance between Ekman transport and damping by air-sea fluxes and radiative adjustment (Spall & Schneider, 2016).

Midlatitude coastal upwelling zones are often found to be regions of model-data mismatch (Dowsett et al., 2012; Fedorov et al., 2013; Feng et al., 2020; McClymont et al., 2020), and several ideas have been suggested to explain

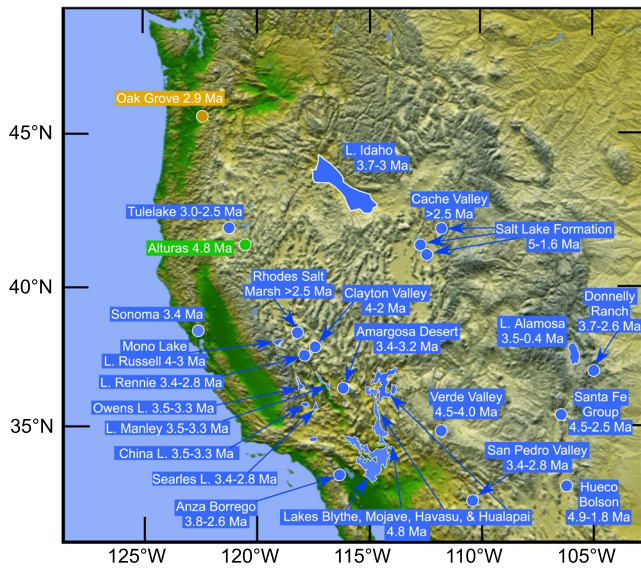


**Figure 1.** Topographic map of the western United States showing Pliocene lakes and other sites where lacustrine deposits or fossil finds indicate wetter environments than today. Pollen and megafossil fossils call for a drier environment than today at Oak Grove, but wetter at Cache Valley and Sonoma (e.g., Minnich, 2007; Thompson, 1991; Thompson & Fleming, 1996; Wolfe, 1990). Abundant lacustrine sediment with fish fossils and pollen suggestive of moist environments attest to a large lake, Lake Idaho, that had formed before 3.7 Ma and lingered until ~3 Ma (e.g., Forester, 1991; Leopold & Wright, 1985; Smith, 1987; Smith & Patterson, 1994; Thompson, 1996). Diatoms, pollen, and ostracods attest to a wetter environment in Tulelake than today (Adam et al., 1989, 1990; Thompson, 1991), but ostracods and other organisms in lacustrine sediment dated to 4.8 at Alturas suggest little difference from today (Forester, 1991). Pliocene lacustrine sediment, in some cases with pollen, mega-plant fossils, and fossils of animals, suggestive of environments wetter than those today, have been reported from numerous inland sites: the Salt Lake Formation in Lake Bonneville cores (Davis & Moutoux, 1998; Kowalewska & Cohen, 1998; Thompson, 1991) and Cache Valley (Brown, 1949; Thompson, 1991; Wolfe, 1990); Rhodes Salt Lake, Clayton Valley, and Lakes Russell and Rennie (Reheis et al., 2002); Verde Valley (Forester, 1991; Thompson, 1991); Donnelly Ranch (Hager, 1974; Thompson, 1991), Santa Fe Group in the Rio Grande Rift (Bartolino & Cole, 2002; Brister & Gries, 1994; Connell et al., 2013; Galusha & Blick, 1971), and Hueco Bolson (Collins & Raney, 1994; Stuart & Willingham, 1984). Hay et al. (1986) used the chemistry of caliche and related deposits to infer marshland and ponds in the Amargosa Desert, as did G. A. Smith (1994); Smith et al. (1993) for the San Pedro Valley. A large lake occupied the Alamosa Basin throughout much of Pliocene and Quaternary time (Machette et al., 2013). Knott et al. (2018) showed shorelines of a number of Pliocene Lakes in the Death Valley-Owens Valley region: Lake Russell, the predecessor to Mono Lake, Lake Manley, Owens, China, Searles Lakes, and other small lakes. Spencer et al. (2013) reported widespread lacustrine sediment that seemed to occupy a series of early Pliocene lakes (Blythe, Mojave, Havasu, and Hualapai) along the modern Colorado River valley in California-Arizona. Petrified wood from the Anza Borrego Desert suggests a wetter climate there (Remeika et al., 1988).

the anomalously warm Pliocene SSTs in these regions. One idea is that the SST anomalies in these regions could have been due to weaker upwelling winds caused by a different large-scale Pliocene SST (Arnold & Tziperman, 2016; Li et al., 2019), or by a wetting of the coastal areas near these upwelling zones (Fu et al., 2021). Alternatively, a deeper thermocline would inhibit the upwelling of deeper, colder water (Boccaletti et al., 2004; Philander & Fedorov, 2003), although a study using an idealized ocean model that resolves the coastal upwelling system suggests that weaker winds are also necessary (Miller & Tziperman, 2017). Model-data mismatches along coastal upwelling zones may be related to insufficient model resolution, as high model resolution in both the atmospheric and ocean components is necessary to accurately simulate upwelling systems (Capet et al., 2004; Gent et al., 2010; Grodsky et al., 2012; Kurian et al., 2021; Miller & Tziperman, 2017; Small et al., 2015).

Over land, there exists geological evidence of wetter subtropical land conditions throughout the Pliocene. Western North America was wetter, with sedimentary evidence of large perennial lakes in Colorado (Machette et al., 2013), Southwestern Idaho (Forester, 1991), and the Death Valley and Lower Colorado River regions of eastern California (Knott et al., 2008; Knott et al., 2018; G. I. Smith, 1984). Paleobotanic evidence also indicates higher levels of rainfall to the south of the Oregon-California border (Thompson, 1991; Thompson & Fleming, 1996). Figure 1 shows a map summarizing evidence of Pliocene lakes over the western United States (the figure appears as Figure S1 in Fu et al., 2021). Overall, global climate was characterized by wetter subtropical continents, with many modern-day subtropical desert regions apparently far less arid during Pliocene time (Burls & Fedorov, 2017; Pound et al., 2014; Salzmann et al., 2008). For a more comprehensive summary of the global geological evidence, see Fu et al. (2021) and references therein. Previously proposed explanations for wetter Pliocene conditions over the subtropics include atmospheric teleconnections from a warmer Eastern Equatorial Pacific (the so-called “permanent El Niño” mechanism mentioned above; Ibarra et al., 2018; Molnar & Cane, 2002, 2007; Winnick et al., 2013). Other studies have additionally considered the role of reduced zonal and meridional SST gradients, which can lead to Hadley cell weakening and reduced moisture divergence over the subtropics (Burls & Fedorov, 2017). Searles (2008) performed a modeling study that prescribed SST warmth along coastal regions and found wetter environments adjacent to all four present-day eastern boundary currents. They used an older and coarser atmospheric model and did not examine the seasonal structure of the precipitation enhancement nor its mechanisms.

In this article, we investigate the effect of warm coastal SSTs near upwelling zones on the hydroclimate over the adjacent subtropical continent. Neither coupled General Circulation Models (GCMs) forced by Pliocene-like boundary conditions (Dowsett et al., 2012; Fedorov et al., 2013; Feng et al., 2020), nor commonly used full-field reconstructions of Pliocene SSTs (e.g., the Pliocene Research, Interpretation and Synoptic Mapping project; Dowsett & Robinson, 2009) reflect marked warmth along subtropical coastal upwelling regions, although such warmth is seen in some proxy records from studies done at individual Ocean Drilling Program (ODP) sites, such as Site 1012 (Brierley et al., 2009), Site 1014 (Dekens et al., 2007), and Sites 1010 & 1021 (LaRiviere et al., 2012). We will therefore explore the implications of SST warming along the California coast to climate over western North America by prescribing plausible patterns of warmth along the California Current in an atmospheric GCM. We demonstrate that the inclusion of enhanced coastal SST warming leads to increased rainfall over the nearby

southwestern United States, helping to reconcile the wetter Pliocene subtropical conditions with projections of 21st century drying (Seager et al., 2007; Seager & Vecchi, 2010).

In Section 2, we introduce our methodology, including model configuration and procedure for prescribing coastal SST warming. Section 3 describes our results, including analysis of the atmospheric moisture budget and storm tracks. We conclude and discuss implications for the understanding of Pliocene climate in Section 4.

## 2. Methods

### 2.1. Model Configuration

For our study, we use the NCAR Community Earth System Model (CESM) version 1.2.2.1 with the Community Atmosphere Model version 5.3 as the atmospheric component (Neale et al., 2012). The Community Land Model version 4.0 (D. M. Lawrence et al., 2011) is used, with all orbital parameters set to modern values; bulk aerosols are prescribed and the chemistry package is disabled. All simulations are run at approximately  $1^\circ$  horizontal resolution ( $0.9^\circ \times 1.25^\circ$ ) with 30 vertical levels. Modern topography, a reasonable approximation for Pliocene values, and modern land surface types, are used in all simulations for simplicity. All simulations are run for 100 yr, with the initial 5 yr discarded to allow for spin-up.

A simulation representing modern-day conditions (experiment Modern) is run with a  $\text{CO}_2$  concentration of 355 ppm and prescribed HadISST SSTs (Hurrell et al., 2008), whereas a simulation representing Pliocene conditions (experiment PRISM) is run at a presumed Pliocene  $\text{CO}_2$  concentration of 405 ppm (Haywood et al., 2010), with prescribed SSTs from PRISM3 representative of mid-Piacenzian conditions (Dowsett & Robinson, 2009). Next, we perform two simulations, as in experiment PRISM, except with modified SST boundary conditions. In these experiments, SSTs along the California margin are adjusted to more closely match early-to mid-Pliocene SSTs inferred at ODP sites 1010, 1012, 1014, and 1021 (experiments  $\text{PRISM}_{135\text{W}}$  and  $\text{PRISM}_{150\text{W}}$ ).

### 2.2. SST Modification

Both HadISST (representing modern conditions) and PRISM3 SSTs are characterized by a relatively broad southward intrusion of cold SSTs off the coast of California (Figures 2a and 2b). This pattern is associated with the California Current, an Eastern Boundary Current flowing southward along the west coast of North America. The current is associated with cold surface temperatures due to a combination of alongshore advection of subarctic waters, offshore Ekman transport leading to upwelling of cold subsurface waters, as well as positive wind stress curl leading to additional upwelling farther offshore from the near-coastal strip. The fact that proxy reconstructions of the early-to mid-Pliocene SST along the California coast show temperature differences of as much as  $+9^\circ\text{C}$  (Brierley et al., 2009; Dekens et al., 2007; LaRiviere et al., 2012) indicates that this southward intrusion of cold SSTs may have been much weaker, if not absent, during the early-to mid-Pliocene.

We begin with the PRISM3 SST (Figure 2a). For each month in this data set, the meridional SST profile at the  $135^\circ\text{W}$  meridian is obtained for the  $\text{PRISM}_{135\text{W}}$  experiment, and at the  $150^\circ\text{W}$  meridian for  $\text{PRISM}_{150\text{W}}$ . SSTs to the east of this meridian, if lower, are replaced by their corresponding value at the same latitude; otherwise they remain unchanged. This procedure is performed starting from  $135^\circ\text{W}/150^\circ\text{W}$  eastward to the California coast between the latitudes of  $10^\circ\text{N}$  and  $60^\circ\text{N}$ . This generates two modified SST patterns that are virtually independent of longitude over the eastern part of the subtropical Eastern Pacific (Figure 2a, white contours) and unchanged over the rest of the Earth.

The SST differences resulting from the procedure described above are largest around  $35^\circ\text{N}$  near the coast, but they decay offshore over a scale hundreds of km (Figures 2c and 2d). The resulting SST difference for  $\text{PRISM}_{150\text{W}}$  is larger in magnitude and spatial scale than for  $\text{PRISM}_{135\text{W}}$ , as the contours are flattened starting from farther offshore. The annual-mean SST difference between PRISM and Modern near the location of ODP Site 1014 off the California margin without modification is around  $+2^\circ\text{C}$ ; the adjustment performed here results in a total SST difference of around  $+6^\circ\text{C}$  between  $\text{PRISM}_{150\text{W}}$  and Modern and  $+4.5^\circ\text{C}$  between  $\text{PRISM}_{135\text{W}}$  and Modern, making the SST field more consistent with the approximately  $+7^\circ\text{C}$ – $-9^\circ\text{C}$ -SST difference inferred from proxy reconstructions during the early-to mid-Pliocene (Brierley et al., 2009; Dekens et al., 2007; LaRiviere et al., 2012). The plausibility of the prescribed SST patterns will be discussed further in Section 4.

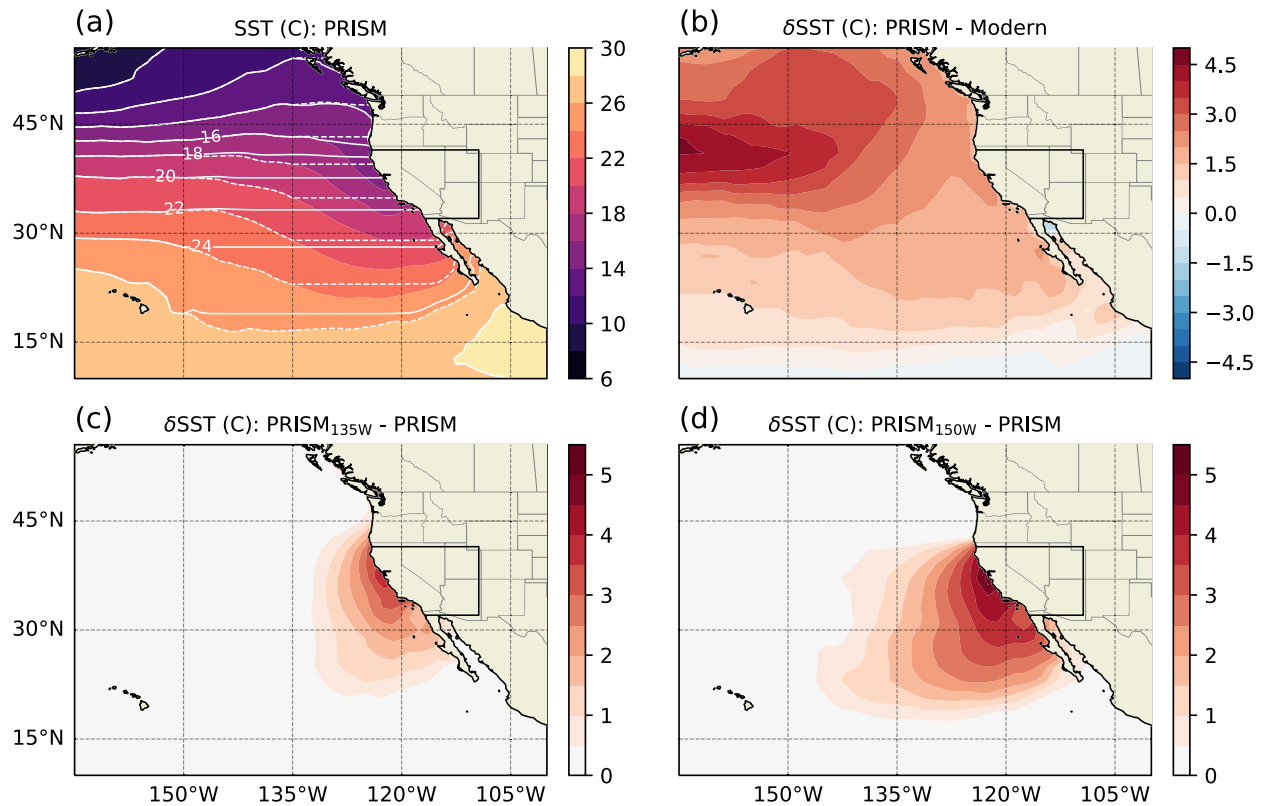


**Figure 2.** (a) Annual mean PRISM SST (shading), PRISM<sub>150W</sub> SST (solid white contours), and PRISM<sub>135W</sub> SST (dashed white contours). (b) Difference between PRISM and Modern SST. (c) Difference between PRISM<sub>135W</sub> and PRISM SST. (d) Difference between PRISM<sub>150W</sub> and PRISM SST.

### 2.3. Reanalysis

For model-data intercomparison, we use monthly averaged precipitation and evaporation fields from the ERA-5 global reanalysis (Hersbach et al., 2020) over the period of 1979–2019.

## 3. Results

Increased coastal temperatures are found to have a wetting effect on the southwestern USA. The prescribed coastal SST warming is sufficient to transform regions of hyperaridity to potential watershed areas characterized by small, but positive precipitation minus evaporation ( $P - E$ ) values. We proceed by first analyzing the annual mean hydrological cycle, and then studying monthly and seasonal rainfall. To better understand the cause of the precipitation differences, we also study the atmospheric moisture budget and midlatitude cyclone tracks.

### 3.1. Annual-Mean Precipitation

Figure 3a shows the annual-mean precipitation over North America in the Modern experiment. In this simulation, much of the southwestern USA receives less than 1 mm/day rainfall on average. As a result, there exist near-zero or negative values of precipitation minus evaporation ( $P - E$ ) over these areas, corresponding to extreme aridity. Precipitation differences between PRISM and Modern are positive south of 30°N, as shown in Figure 3b. Over the southwestern USA, however, differences are small and not of consistent sign, with negative values along the California coast. The large-scale SST differences between PRISM and Modern are therefore not sufficient to explain the wetter Pliocene conditions inferred over much of western North America. A comparison of annual-mean climatologies between the Modern CESM simulation and ERA5 reanalysis is also provided in Figure S1 in Supporting Information S1, showing that CESM reproduces the observed annual-mean precipitation and  $P - E$  patterns over this region.

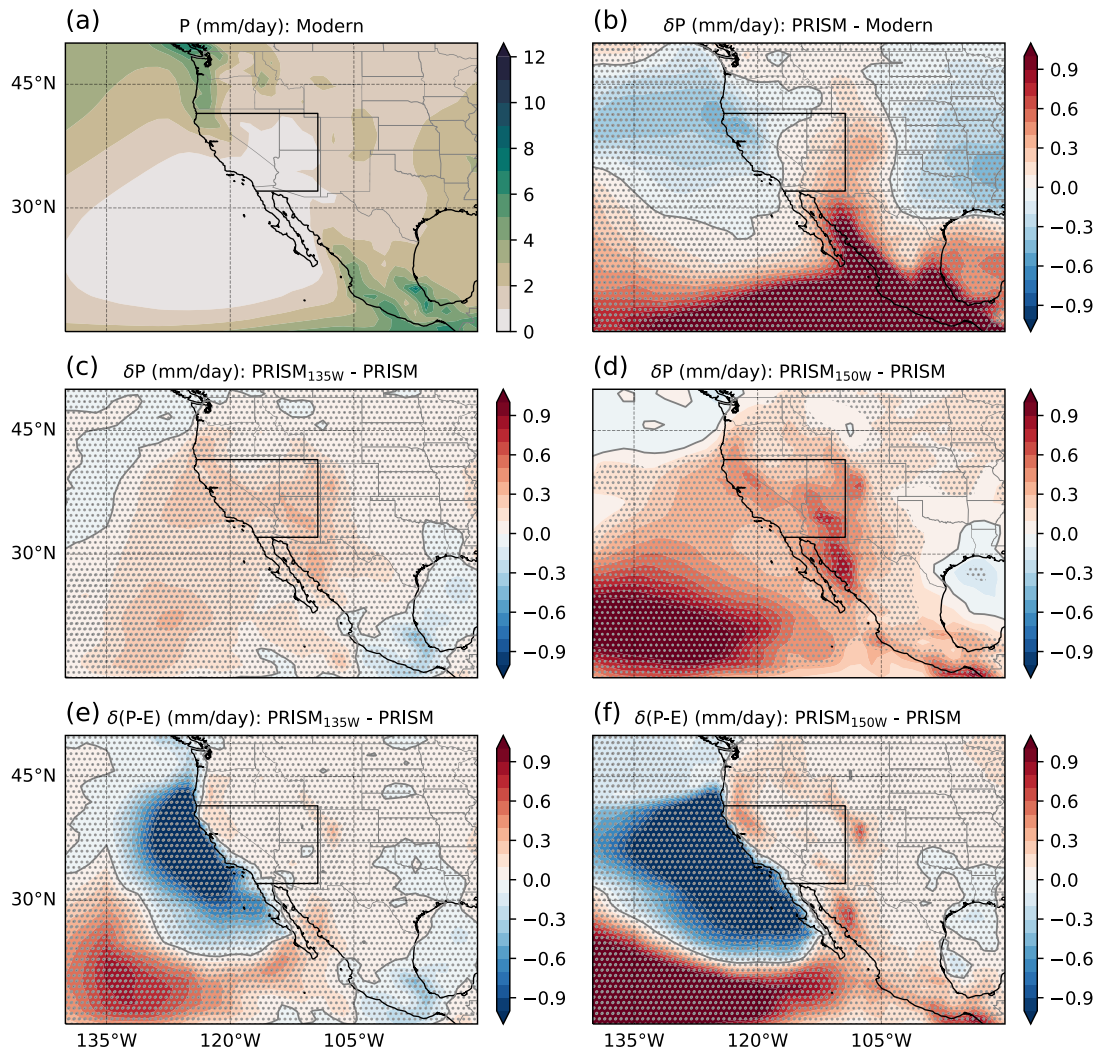


**Figure 3.** (a) Annual mean Modern precipitation over North America. (b) Precipitation difference between PRISM and Modern. (c) Precipitation difference between PRISM<sub>135W</sub> and PRISM. (d) Precipitation difference between PRISM<sub>150W</sub> and PRISM. (e, f) As in (c, d), but for differences in  $P - E$  rather than  $P$ . Stippling indicating differences significant to a 95% confidence level from the two-tailed  $t$  test. Southwest Region (SWR) shown by the solid black contour over land.

When warmer SSTs are prescribed along the coast (experiments PRISM<sub>135W</sub> and PRISM<sub>150W</sub>), rainfall increases  $\sim 20\%$ – $40\%$  over the southwestern USA, with some regions receiving an extra 0.5–1 mm/day of precipitation (Figures 3c and 3d). The region of statistically significant rainfall increase is large in extent and covers most of the areas where Pliocene lakes were inferred (Figure 1). Furthermore, the excess precipitation leads to increased  $P - E$  over much of western North America (Figures 3e and 3f). PRISM<sub>135W</sub>, the experiment with a smaller SST increase, leads to differences of smaller magnitude compared to PRISM<sub>150W</sub>, but of a similar spatial pattern. The mechanisms for increased precipitation caused by the prescribed coastal warming turn out to differ between summer and winter, so we next consider monthly rainfall over the southwestern USA.

### 3.2. Monthly Precipitation

Rainfall in the southwestern USA is known to vary seasonally (e.g., rainfall associated with the North American Monsoon; Adams & Comrie, 1997), so we investigate the seasonality of rainfall and evaporation in our experiments. To analyze monthly rainfall, we define a domain, referred to as the Southwest Region (hereafter referred to as the SWR). It is a box extending meridionally from 32°N to 41°N, and bounded by the 110°W meridian on the east, and the California coast on the west. The SWR is visualized by the solid black contour over land in Figure 3.

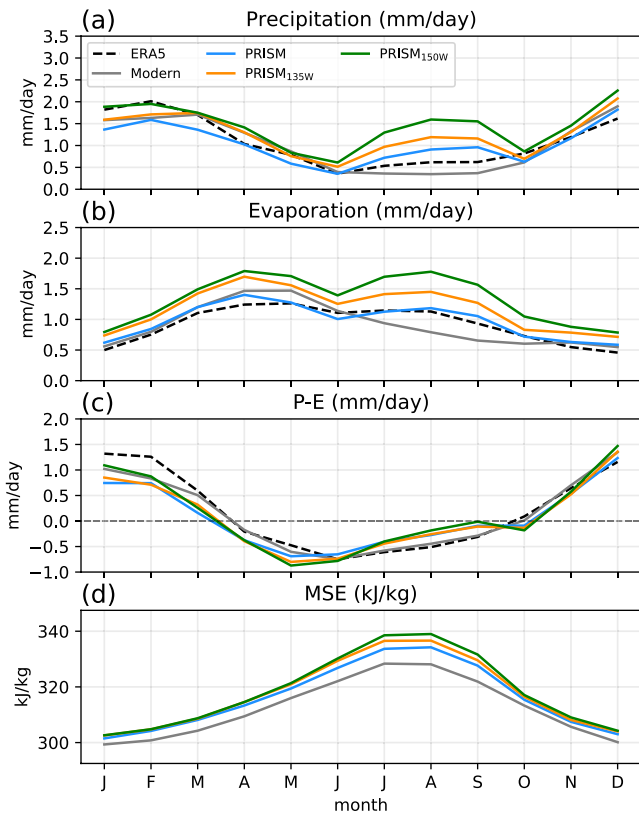


**Figure 4.** Seasonal hydrological cycle over the Southwest Region (SWR, as shown by the solid black contour in Figure 3). ERA5 reanalysis shown in the dashed black curve. (a) Monthly average precipitation rate over the SWR. (b–d) As in (a), but for evaporation rate,  $P - E$ , and surface moist static energy (MSE) over the SWR respectively.

We plot in Figure 4a the seasonal variation in rainfall averaged over the SWR. The seasonal precipitation from ERA5 reanalysis is also included for comparison in the dashed black curve. Compared to Modern, PRISM shows increased summertime rainfall but reduced precipitation over winter and spring. As we will show shortly, this is due to differences in storm tracks and summertime moisture convergence. The annual-mean rainfall, however, does not differ significantly over this region between PRISM and Modern. Compared to PRISM, the PRISM<sub>135W</sub> and PRISM<sub>150W</sub> simulations show elevated precipitation rates throughout the year (of around 20% and 40% respectively), with the largest increases over late boreal summer. Due to the high potential evapotranspiration over the arid Southwest, evaporation rises accordingly when elevated precipitation occurs (Figure 4b). It is possible that the large-scale atmospheric moisture divergence, influenced by the SST, also contributes to increased evaporation. However, the net effect is characterized by increased  $P - E$  associated with warmer SSTs offshore (Figure 4c), especially during the summer and winter seasons, and is consistent with the statistically significant differences shown in Figures 3e and 3f.

### 3.3. Moisture Budget

To investigate the mechanisms behind precipitation minus evaporation ( $P - E$ ) differences quantitatively, consider the time-averaged atmospheric moisture budget:

$$\overline{P} - \overline{E} = -\frac{1}{g\rho_w} \nabla \cdot \int_0^{p_s} \overline{q\vec{v}} dp. \quad (1)$$

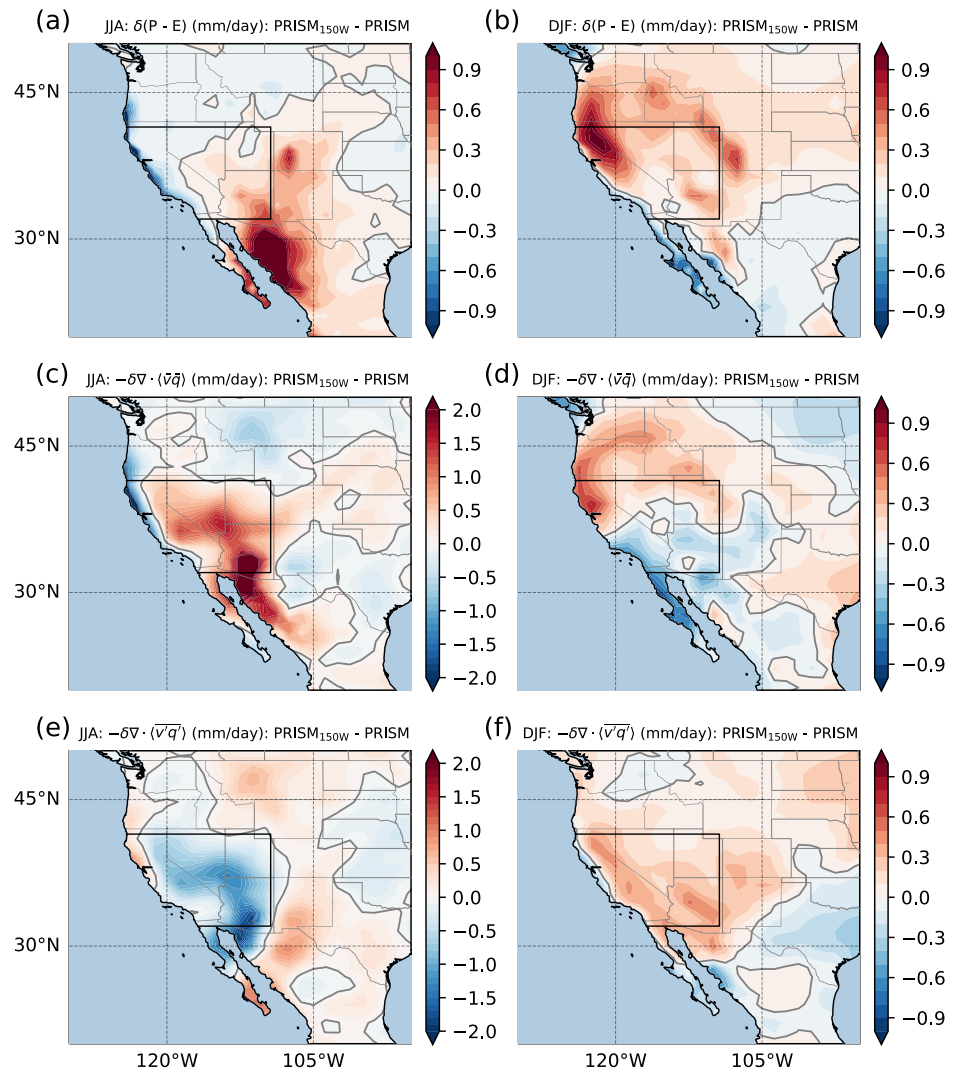
In this equation, the overbar refers to a temporal average,  $p_s$  is the surface pressure,  $\vec{v}$  is the horizontal wind,  $g$  is the gravitational acceleration, and  $\rho_w$  is the density of water. This equation states that averaged over time, precipitation minus evaporation in an atmospheric column must be balanced by the column-integrated convergence of moisture. We proceed by evaluating the June–July–August (JJA) and December–January–February (DJF) moisture budgets individually.

The difference in moisture convergence between PRISM<sub>150W</sub> and PRISM is plotted in Figure 5a for JJA. Differences in the RHS of Equation 1, denoted as  $-\nabla \cdot \langle q\vec{v} \rangle$  (where  $\langle * \rangle \equiv 1/(g\rho_w) \cdot \int_0^{p_s} * dp$ ), are found to match the spatial pattern of  $\overline{P} - \overline{E}$ , with agreement in sign over most areas. The mismatches, which may arise from the calculation of divergences using centered finite differences, are shown in Supporting Information S1. The similar spatial pattern and general agreement in sign indicate that the atmospheric moisture budget is sufficiently closed for the purposes of this study. We proceed to separate the right-hand side of Equation 1 into its mean and eddy components:

$$-\frac{1}{g\rho_w} \nabla \cdot \int_0^{p_s} \overline{q\vec{v}} dp = -\frac{1}{g\rho_w} \nabla \cdot \int_0^{p_s} \overline{q\vec{v}} dp - \frac{1}{g\rho_w} \nabla \cdot \int_0^{p_s} \overline{q'\vec{v}'} dp. \quad (2)$$

The first term on the RHS of Equation 2 represents the convergence of moisture by the mean flow (hereafter referred to as “mean convergence”), whereas the second term corresponds to the convergence of moisture by eddy fluxes (hereafter referred to as “eddy convergence”). Next, we use Equation 2 to diagnose  $\overline{P} - \overline{E}$  differences. During the boreal summer, much of the  $\overline{P} - \overline{E}$  difference between PRISM<sub>150W</sub> and PRISM in the southwestern USA is related to enhanced mean convergence (Figure 5c), and eddy convergence for PRISM<sub>150W</sub> is smaller than that for PRISM (Figure 5e). The overall spatial pattern is dominated by enhanced  $P - E$  over Mexico and the American Southwest, with reductions in  $P - E$  north of around 40°N (Figure 5a).

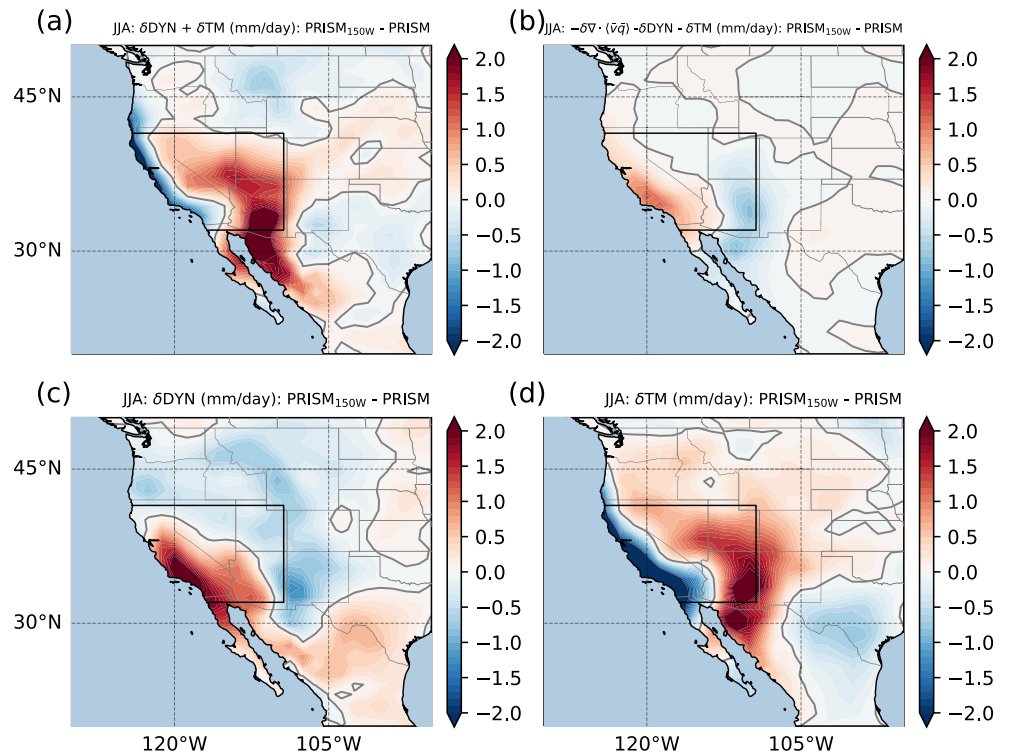
Given the dominance of the difference in mean moisture convergence for the JJA moisture budget (Figure 5c), we further decompose the difference in mean moisture convergence into its dynamic and thermodynamic components as follows:



**Figure 5.** Decomposition of the atmospheric moisture budget into mean and eddy terms, defined in Equation 2. (a) Difference in  $\bar{P} - \bar{E}$  between PRISM<sub>150W</sub> and PRISM over June-July-August (JJA). (b) As in (a), but for December-January-February (DJF). (c) Difference in the mean moisture convergence over JJA. (d) As in (c), but for DJF. (e) Difference in eddy moisture convergence over JJA. (f) As in (e), but for DJF. Colorbar limits in panels (c and e) differ from those in other panels.

$$-\delta \left( \frac{1}{g\rho_w} \nabla \cdot \int_0^{p_s} \bar{q} \bar{v} dp \right) \approx -\frac{1}{g\rho_w} \nabla \cdot \int_0^{p_s} \bar{q} \delta \bar{v} dp - \frac{1}{g\rho_w} \nabla \cdot \int_0^{p_s} \bar{v} \delta \bar{q} dp \quad (3)$$

where  $\delta$  represents the difference between the PRISM<sub>150W</sub> and PRISM experiments, and differences in horizontal wind and specific humidity are assumed to be small compared to the mean. The first term on the right hand side of Equation 3 reflects differences in moisture convergence caused by changes in the horizontal wind field, and will be called the dynamic component ( $\delta$ DYN). The second term, which is driven by differences in specific humidity, is called the thermodynamic component ( $\delta$ TH). A plot of the sum of  $\delta$ DYN and  $\delta$ TH, a comparison of the sum to the mean convergence, and  $\delta$ DYN and  $\delta$ TH shown separately is provided in Figure 6. The decomposition of the mean convergence into two terms shows that the dynamic component plays a role in enhanced mean moisture convergence near the coast (Figure 6c), whereas the thermodynamic process is dominant further inland (Figure 6d). Dynamically, the increased mean convergence over the SWR can be attributed to enhanced summertime convection. This is related to the enhanced surface moist static energy (MSE) over the region (Figure 4d), which reflects reduced atmospheric stability and more favorable conditions for low-level convergence (Emanuel, 1994).



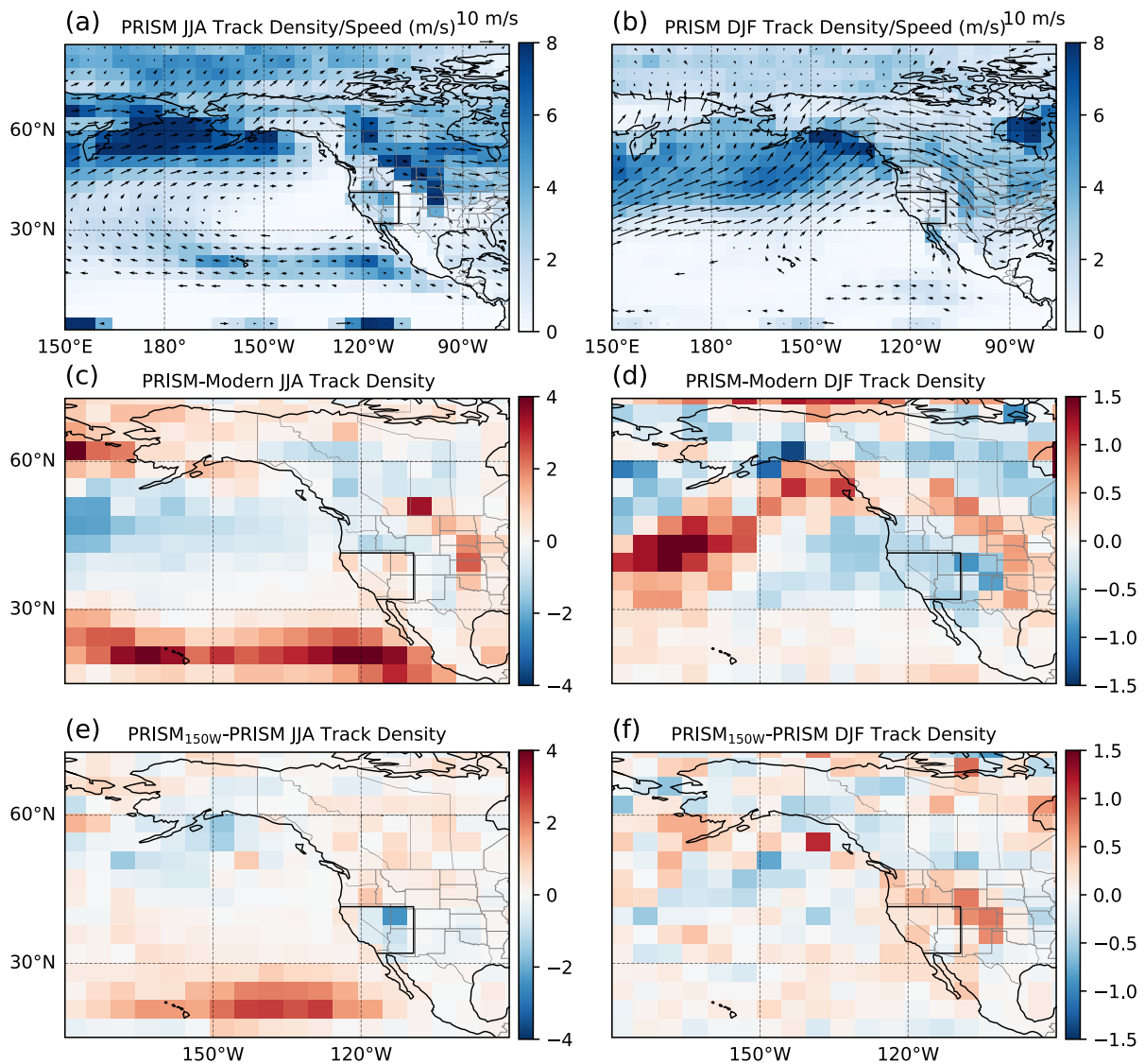
**Figure 6.** Decomposition of the difference in JJA mean moisture convergence between  $PRISM_{150W}$  and PRISM into dynamic ( $-\nabla \cdot \langle \bar{q} \delta \bar{v} \rangle$ ) and thermodynamic ( $-\nabla \cdot \langle \bar{v} \delta \bar{q} \rangle$ ) components. (a) Sum of  $\delta DYN$  and  $\delta TM$ , which is approximately equal to  $-\delta V \cdot \langle \bar{v} \bar{q} \rangle$  as shown in Figure 5c. (b) Residual between  $-\delta V \cdot \langle \bar{v} \bar{q} \rangle$  and the sum of  $\delta DYN$  and  $\delta TM$ . (c) Dynamic component of the difference in mean moisture convergence ( $\delta DYN$ ). (d) Thermodynamic component of the difference in mean moisture convergence ( $\delta TM$ ).

Figure 5b shows  $\bar{P} - \bar{E}$  differences averaged over DJF. The spatial pattern of  $\delta(\bar{P} - \bar{E})$  during DJF is quite different from JJA, with moistening observed from roughly 30°N to 50°N. Regions south of 30°N, including much of Mexico, are instead characterized by reduced  $\bar{P} - \bar{E}$ . Decomposition of moisture convergence into its mean and eddy components shows greater mean convergence over Northern California and the Pacific Northwest in  $PRISM_{150W}$  than PRISM, but less than that for PRISM over most of the southwestern USA and northwestern Mexico. DJF eddy convergence for  $PRISM_{150W}$ , however, is greater than that for PRISM over nearly all of western North America, except for some regions over parts of Mexico and farther east. Therefore, the greater winter rainfall over the southwestern USA in  $PRISM_{150W}$  than PRISM can be mainly attributed to greater *eddy* moisture convergence. Similar differences, of smaller magnitude, are seen in the  $PRISM_{135W}$  experiment (Figure S3 in Supporting Information S1). The residual between  $\bar{P} - \bar{E}$  and moisture convergence for  $PRISM_{135W}$  is shown in Figure S4 in Supporting Information S1.

### 3.4. Track Analysis

Increased eddy convergence during winter suggests that midlatitude cyclones may play an important role in excess wintertime precipitation. We perform feature tracking of atmospheric cyclone trajectories using TRACK, an objective feature detection algorithm. TRACK applies a spectral filter to 6-hourly instantaneous sea level pressure (SLP) data by decomposing SLP into spherical harmonics and setting total wave numbers smaller than six to zero (Hodges, 1996). The algorithm then detects filtered trajectories of atmospheric cyclone centers, which are required to persist for at least 1 day and translate at least 1,000 km horizontally. When computing the density of cyclone tracks, cyclone frequencies are normalized by bin area to be in units of  $km^{-2} yr^{-1}$ . This results in a track density estimate that is independent of model resolution.

We first plot the climatological cyclone track densities over JJA (Figure 7a) and DJF (Figure 7b), with track density in shading and mean cyclone trajectory velocity shown in arrows. TRACK is able to detect both tropical



**Figure 7.** (a) JJA cyclone track density and mean cyclone translation velocity for PRISM. (b) As in (a), but for DJF. (c) JJA track density difference between PRISM and Modern simulations. (d) As in (c), but for DJF. (e) JJA track density difference between PRISM<sub>150W</sub> and PRISM simulations. (f) As in (e), but for DJF.

cyclones and midlatitude cyclones; we observe large track densities south of 30°N during JJA, corresponding to trajectories of eastern North Pacific tropical cyclones. As tropical cyclones are shown not to play a major role in the moisture budget over the SWR (Figure 8), we instead focus on midlatitude cyclones, which show considerable differences in their track densities between JJA (Figure 7a) and DJF (Figure 7b). During winter, midlatitude cyclones occur further to the east, near the coast of the Pacific Northwest and their trajectories exhibit a strong northeastward translation over the East Pacific. On the other hand, during JJA, midlatitude cyclones are virtually absent off the coast of western North America and exhibit a much smaller translation speed, thus not playing a major role in the JJA moisture budget.

To verify the role that cyclones play in eddy moisture convergence, we identify the days with precipitation over the SWR exceeding the 95th percentile during JJA and DJF. The track density for cyclones occurring during these 95th percentile precipitation days is computed, and seasonal climatology track density is subtracted away to provide *anomalies* in track densities associated with strong precipitation events in JJA (Figure 8a) and DJF (Figure 8b). The same procedure is performed for PRISM (Figures 8c and 8d) and PRISM<sub>150W</sub> (Figures 8e and 8f). Superimposed on Figure 8 is the anomaly surface wind field (arrows) during the 95th percentile precipitation days. The results show that wintertime precipitation over the southwestern USA is associated with cyclonic circulation

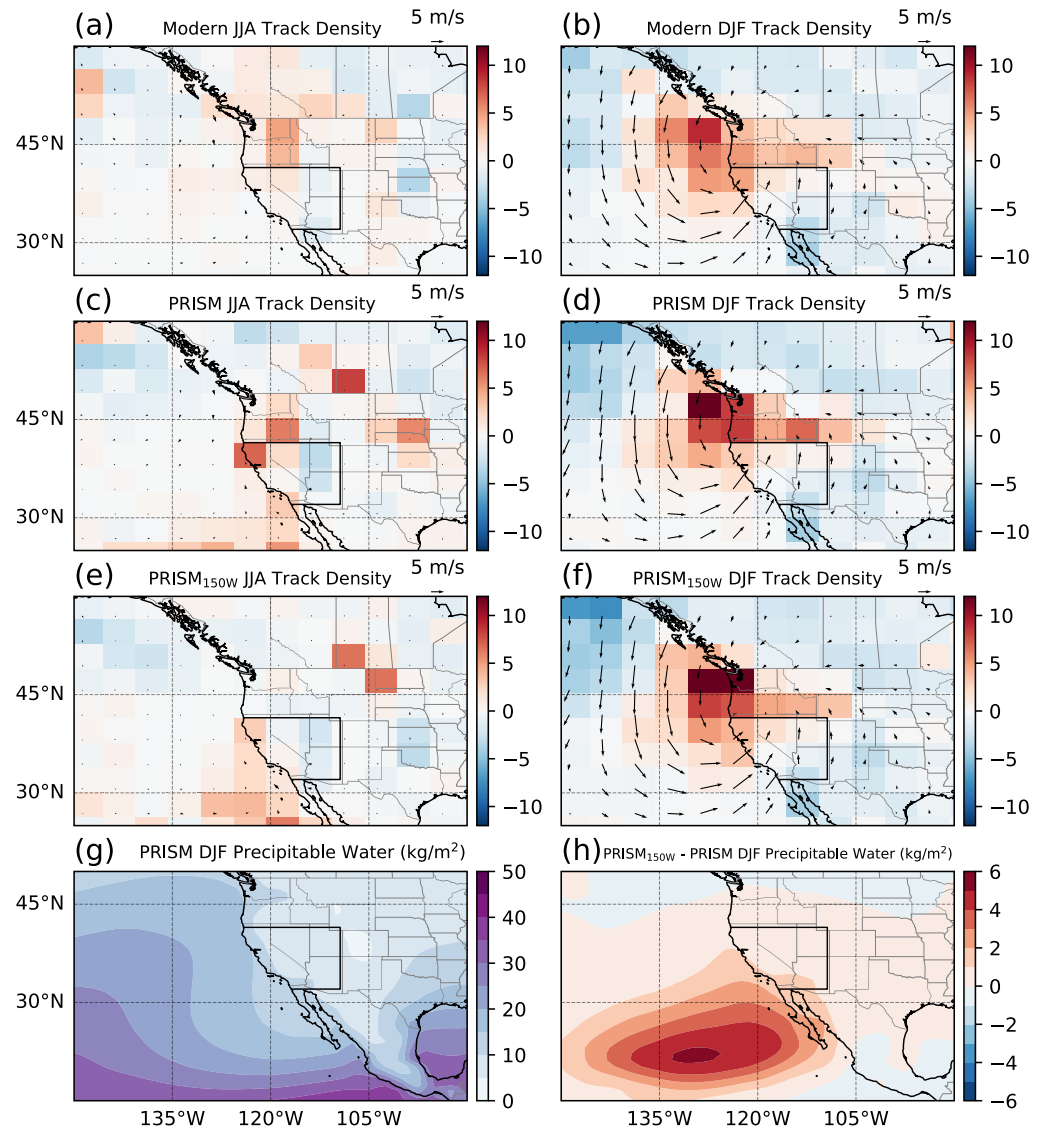


**Figure 8.** (a) Anomaly surface wind field (arrows) and anomaly cyclone track density during 95th-percentile precipitation days over the SWR for JJA. (b) As in (a), but for DJF. (c–d) As in (a–b), but for PRISM. (e–f) As in (a–b), but for PRISM<sub>150W</sub>. (g) Vertically integrated precipitable water for PRISM for DJF. (h) Difference in vertically integrated precipitable water for DJF between PRISM<sub>150W</sub> and PRISM.

and elevated track densities over the Pacific Northwest around 45°N and 120°W. The surface wind field associated with these cyclones is perpendicular to shore along the California coast (Figure 8b), such that the cyclones advect moister offshore parcels toward the continental interior. On the other hand, summertime precipitation is not clearly attributable to either midlatitude or tropical cyclones. This is consistent with Figure 5, which showed that increased summer precipitation is caused by higher mean, rather than eddy convergence.

Compared to Modern, wintertime midlatitude cyclone tracks for PRISM are shifted polewards (Figure 7d). This explains why in Figure 4a, wintertime precipitation is lower in PRISM compared to Modern (and in projections of future climates, e.g., Seager & Vecchi, 2010). During the summer, more tropical cyclones occur in PRISM<sub>150W</sub> compared to PRISM (Figure 7e) over the subtropical Eastern Pacific. These, however, are not expected to strongly affect the moisture budget. During the winter, slightly more cyclones occur in PRISM<sub>150W</sub> compared to PRISM around the Pacific Northwest, in the region associated with 95th percentile precipitation events (Figure 8b). Perhaps more importantly, these storms advect surface air parcels onshore from the region of elevated SSTs, characterized by higher specific humidity by the Clausius-Clapeyron relation (Figures 8g and 8h). The increased

column moisture and higher storm track density help explain the enhanced eddy convergence shown in Figure 5f that is responsible for greater DJF precipitation for PRISM<sub>150W</sub> than PRISM.

#### 4. Discussion and Conclusions

We have shown that SST warmth prescribed over relatively restricted regions off the coast of the California margin are sufficient to increase precipitation over southwestern North America. We first show that PRISM3, a commonly used Pliocene SST proxy reconstruction, when used to force an atmospheric GCM, does not simulate significantly increased precipitation over southwestern North America as was inferred from observations (Forester, 1991; Knott et al., 2008; G. I. Smith, 1984; Thompson, 1991; Thompson & Fleming, 1996). When coastal SSTs are raised to values in better agreement with proxy reconstructions, much of western North America receives increased mean rainfall throughout the year. In particular, over the southwestern USA, a large monsoonal precipitation anomaly develops during late boreal summer in response to increased surface MSE and results in enhanced summertime mean atmospheric moisture convergence. During the winter, rainfall increases slightly, and instead results from an increased number of cyclones off the coast of the Pacific Northwest, which also advect more moisture onshore. The annual-mean precipitation differences due to the raised coastal SSTs are sufficient to transform regions of the southwestern USA from regions of hyperaridity, like that at present, to regions characterized by small, but positive  $P - E$ , which may better support the vegetated ecosystems and wetter land types that existed during the Pliocene. The results we found are consistent with the annual-mean results shown in the earlier modeling study by Searles (2008). They are also consistent with the correlation of rainfall over the western US with the warm phase of the Pacific Decadal Oscillation, a mode of natural variability associated with warm SSTs along the California coast (Mantua & Hare, 2002).

Fu et al. (2021) demonstrated that wetter subtropical conditions along the coast can lead to weaker alongshore upwelling-favorable winds, helping to explain anomalously warm Pliocene coastal SSTs. Here, we have shown that likewise, warmer coastal temperatures can moisten the land along the continental margin. Together, these represent a potential feedback between weakened upwelling and enhanced rainfall over the coast. This feedback may act to further enhance the hydrological effects associated with a “permanent El Niño” (Ibarra et al., 2018; Molnar & Cane, 2002, 2007; Winnick et al., 2013) or reduced Pliocene meridional SST gradients (Burls & Fedorov, 2017). Although land types are prescribed in our simulations, the increased rainfall may facilitate the development and sustaining of wetter land types (e.g., lakes and wetlands, Ibarra et al., 2018). These land types would then further suppress coastal upwelling.

The two SST warming patterns that we have prescribed are consistent with the proxy evidence and are seemingly plausible. In combination with the subtropical PRISM SST warming of around  $+2^{\circ}\text{C}$ , the SST is raised by around  $+6^{\circ}\text{C}$  in total along the California coast compared to Modern in the PRISM<sub>150W</sub> experiment, and by  $+4.5^{\circ}\text{C}$  in PRISM<sub>135W</sub>. We note that SST reconstructions from sediment cores reflect point measurements, so the complete spatial pattern of SST differences is unclear. However, coastal upwelling is known to affect SST hundreds of kilometers offshore through Ekman transport (Spall & Schneider, 2016). Furthermore, the anomalous warmth at the ODP sites has been difficult to explain via wind and stratification differences alone (Miller & Tziperman, 2017). It seems likely that additional processes, such as a weakened California current advecting less high latitude colder waters, or radiative feedbacks, including cloud radiative forcing, may have also contributed to Pliocene warmth over these regions. These mechanisms would be associated with larger spatial scales of SST warming, supporting the patterns of warming that we have prescribed.

We remark that some studies targeting the mid-Piacenzian have shown a smaller warm signal along the California coast (e.g., Foley & Dowsett, 2019; Herbert et al., 2016). Furthermore, simulations from the Pliocene Model Intercomparison Project now show improved data-model agreement along the California current (Haywood et al., 2020) when compared to Foley and Dowsett (2019). Given uncertainties in interpreting alkenone-based SSTs (e.g., Leduc et al., 2014), it is possible that the prescribed SST differences we have prescribed could be overestimated. In that case, the proposed mechanism may be less relevant.

SST proxies are tied to biological productivity, and it is possible that proxy reconstructions better reflect seasonal, rather than annual-mean SSTs. Given that the modern-day upwelling season is considered to occur from approximately May to August (Dorman & Winant, 1995; Halliwell & Allen, 1987), the SST changes that we have prescribed may be most justified over these months. Indeed, the largest precipitation differences we find are from

June to August, overlapping with the modern upwelling season. The fact that the months over which our coastal SST modification appears most justifiable are also the months with the largest difference in southwestern US rainfall agrees with the mechanism presented.

Although the Pliocene is considered a useful analog for understanding anthropogenic climate change, there exist notable differences between inferred Pliocene conditions and future climate projections. Chief among these is the anomalous warmth at mid-latitude coastal upwelling sites, such as off the California coast, where SSTs may have been up to 9°C higher than the present. Global climate models, however, generally do not reflect the warm SSTs inferred at these coastal upwelling sites. Furthermore, when used for future climate predictions, these models typically predict drying over the 21st century rather than a transition to wetter conditions over subtropical desert regions (Burls & Fedorov, 2017; Seager et al., 2007; Seager & Vecchi, 2010). Model-data mismatches in these regions are therefore of special scientific interest, and of societal relevance, due to the ecological and economic importance of coastal upwelling zones and the need for long-term projections of rainfall trends over many parts of the world.

The local feedback suggested here therefore hints at a potential mechanism for explaining differences between decadal-scale drying trends in the southwestern USA (Seager et al., 2007; Seager & Vecchi, 2010) and the wetter environment of the Pliocene, which possibly reflects the conditions of a fully equilibrated high-CO<sub>2</sub> climate. The use of a coupled, rather than atmosphere-only model will be needed to fully explore the feedback between coastal SSTs and onshore conditions described above, although very high ocean model resolution is necessary to accurately simulate coastal upwelling (Gent et al., 2010; Grodsky et al., 2012; Miller & Tziperman, 2017; Small et al., 2015). For the foreseeable future, it may therefore be necessary to use a combination of coarse-resolution GCMs and high-resolution regional models to study the complex interaction between coastal upwelling and regional hydroclimate, and how these mechanisms are expected to change in a warming climate.

## Data Availability Statement

All GCM input files and post-processing scripts are available under <https://doi.org/10.17605/OSF.IO/9WXPQ>.

## Acknowledgments

M.F. thanks Duo Chan and Peter Huybers for helpful discussions. E.T. and M.F. were funded by the NSF Climate Dynamics program (joint NSF/NERC program) grant AGS-1924538, and by NSF Climate Dynamics program, grant AGS-1826635; P.M. is supported by AGS-1740536; M.A.C. is supported by NSF award OCE-1657209. E.T. thanks the Weizmann institute for its hospitality during parts of this work. The authors would like to acknowledge high-performance computing support from Cheyenne (doi:<https://10.5065/D6RX99HX>) provided by NCAR's Computational and Information Systems Laboratory, sponsored by the National Science Foundation.

## References

- Adam, D. P., Bradbury, J. P., Rieck, H. J., & Sarna-Wojcicki, A. (1990). Environmental changes in the Tule Lake Basin, Siskiyou and Modoc Counties, California, from 3 to 2 Myr before present. *US Geological Survey Bulletin*, 1933, 1–13.
- Adam, D. P., Sarna-Wojcicki, A. M., Rieck, H. J., Bradbury, J. P., Dean, W. E., & Forester, R. M. (1989). Tulelake, California: The last 3 Myr. *Paleogeography, Paleoclimatology, Paleoecology*, 72, 89–103. [https://doi.org/10.1016/0031-0182\(89\)90134-x](https://doi.org/10.1016/0031-0182(89)90134-x)
- Adams, D. K., & Comrie, A. C. (1997). The North American monsoon. *Bulletin of the American Meteorological Society*, 78(10), 2197–2213. [https://doi.org/10.1175/1520-0477\(1997\)078<2197:tnam>2.0.co;2](https://doi.org/10.1175/1520-0477(1997)078<2197:tnam>2.0.co;2)
- Arnold, N. P., & Tziperman, E. (2016). Reductions in midlatitude upwelling-favorable winds implied by weaker large-scale Pliocene SST gradients. *Paleoceanography*, 31(1), 27–39. <https://doi.org/10.1002/2015pa002806>
- Bartolino, J. R., & Cole, J. C. (2002). Chapter 3: Geology of the Santa Fe Group aquifer system. *Ground-water resources of the Middle Rio Grande Basin* (pp. 23–40), USGS Water-Resources Circular.
- Boccaletti, G., Pacanowski, R. C., Philander, S., Fedorov, A., & Fedorov, A. V. (2004). The thermal structure of the upper ocean. *Journal of Physical Oceanography*, 34(4), 888–902. [https://doi.org/10.1175/1520-0485\(2004\)034<0888:tsotu>2.0.co;2](https://doi.org/10.1175/1520-0485(2004)034<0888:tsotu>2.0.co;2)
- Brierley, C. M., Fedorov, A. V., Liu, Z., Herbert, T. D., Lawrence, K. T., & LaRiviere, J. P. (2009). Greatly expanded tropical warm pool and weakened Hadley circulation in the early Pliocene. *Science*, 323(5922), 1714–1718. <https://doi.org/10.1126/science.1167625>
- Brister, B. S., & Gries, R. R. (1994). Tertiary stratigraphy and tectonic development of the Alamosa Basin (northern San Luis Basin), Rio Grande rift, south-central Colorado. In G. R. Keller, & S. M. Cather (Eds.), *Basins of the Rio Grande Rift: Structure, stratigraphy, and tectonic setting* (pp. 39–58). Geological Society of America Special Paper 291. <https://doi.org/10.1130/spe291-p39>
- Brown, R. W. (1949). Pliocene plants from Cachee (sic) Valley, Utah. *Journal of the Washington Academy of Sciences*, 39(7), 224–229
- Burls, N. J., & Fedorov, A. V. (2017). Wetter subtropics in a warmer world: Contrasting past and future hydrological cycles. *Proceedings of the National Academy of Sciences*, 114(49), 12888–12893. <https://doi.org/10.1073/pnas.1703421114>
- Capet, X. J., Marchesiello, P., & McWilliams, J. (2004). Upwelling response to coastal wind profiles. *Geophysical Research Letters*, 31(13). <https://doi.org/10.1029/2004GL020123>
- Chaisson, W. P., & Ravelo, A. C. (2000). Pliocene development of the east-west hydrographic gradient in the equatorial Pacific. *Paleoceanography*, 15(5), 497–505. <https://doi.org/10.1029/1999pa000442>
- Collins, E. W., & Raney, J. A. (1994). Tertiary and Quaternary tectonics of the Hueco Bolson, Trans-Pecos Texas, and Chihuahua, Mexico. In G. R. Keller, & S. M. Cather (Eds.), *Tertiary and Quaternary tectonics of the Hueco Bolson, Trans-Pecos Texas, and Chihuahua, Mexico. Basins of the Rio Grande Rift: Structure, stratigraphy, and tectonic setting* (pp. 265–282). Geological Society of America Special Paper 291. <https://doi.org/10.1130/spe291-p265>
- Connell, S. D., Smith, G. A., Geissman, J. W., & McIntosh, W. C. (2013). In M. R. Hudson, & V. J. S. Grauch (Eds.), *Climatic controls on non-marine depositional sequences in the Albuquerque Basin, Rio Grande rift, north-central New Mexico. New perspectives on Rio Grande Rift Basins: From tectonics to groundwater* (Vol. 494, pp. 383–425). Geological Society of America Special Paper.

- Davis, O. K., & Moutoux, T. E. (1998). Tertiary and Quaternary vegetation history of the Great Salt Lake, Utah, USA. *Journal of Paleolimnology*, 19(4), 417–427. <https://doi.org/10.1023/a:1007959203433>
- Dekens, P. S., Ravelo, A. C., & McCarthy, M. D. (2007). Warm upwelling regions in the Pliocene warm period. *Paleoceanography*, 22(3). <https://doi.org/10.1029/2006pa001394>
- Dekens, P. S., Ravelo, A. C., McCarthy, M. D., & Edwards, C. A. (2008). A 5 Myr comparison of Mg/Ca and alkenone paleothermometers. *Geochemistry, Geophysics, Geosystems*, 9(10). <https://doi.org/10.1029/2007gc001931>
- Dorman, C. E., & Winant, C. D. (1995). Buoy observations of the atmosphere along the west coast of the United States, 1981–1990. *Journal of Geophysical Research: Oceans*, 100(C8), 16029–16044. <https://doi.org/10.1029/95jc00964>
- Dowsett, H. J., & Robinson, M. M. (2009). Mid-Pliocene equatorial sea surface temperature reconstruction: A multi-proxy perspective. *Philosophical Transactions of the Royal Society*, 367(1886), 109–125. <https://doi.org/10.1098/rsta.2008.0206>
- Dowsett, H. J., Robinson, M. M., Haywood, A. M., Hill, D. J., Dolan, A. M., Stoll, D. K., et al. (2012). Assessing confidence in Pliocene sea surface temperatures to evaluate predictive models. *Nature Climate Change*, 2(5), 365–371. <https://doi.org/10.1038/nclimate1455>
- Dowsett, H. J., Thompson, R., Barron, J., Cronin, T., Fleming, F., Ishman, S., & Holtz, T., Jr (1994). Joint investigations of the middle Pliocene climate I: Prism paleoenvironmental reconstructions. *Global and Planetary Change*, 9(3–4), 169–195. [https://doi.org/10.1016/0921-8181\(94\)90015-9](https://doi.org/10.1016/0921-8181(94)90015-9)
- Emanuel, K. A. (1994). *Atmospheric convection*. Oxford University Press.
- Fedorov, A. V., Brierley, C. M., Lawrence, K. T., Liu, Z., Dekens, P. S., & Ravelo, A. C. (2013). Patterns and mechanisms of early Pliocene warmth. *Nature*, 496(7443), 43–49. <https://doi.org/10.1038/nature12003>
- Feng, R., Otto-Bliesner, B. L., Brady, E. C., & Rosenbloom, N. (2020). Increased climate response and Earth system sensitivity from CCSM4 to CESM2 in mid-Pliocene simulations. *Journal of Advances in Modeling Earth Systems*, 12(8), e2019MS002033. <https://doi.org/10.1029/2019ms002033>
- Foley, K. M., & Dowsett, H. J. (2019). *Community sourced mid-Piacenzian sea surface temperature (SST) data*. US Geological Survey data release. <https://doi.org/10.5066/P9YP3DTV>
- Forester, R. M. (1991). Pliocene-climate history of the western United States derived from lacustrine ostracodes. *Quaternary Science Reviews*, 10(2–3), 133–146. [https://doi.org/10.1016/0277-3791\(91\)90014-1](https://doi.org/10.1016/0277-3791(91)90014-1)
- Fu, M., Cane, M. A., Molnar, P., & Tziperman, E. (2021). Wetter subtropics lead to reduced Pliocene coastal upwelling. *Paleoceanography and Paleoclimatology*, 36(10), e2021PA004243. <https://doi.org/10.1029/2021pa004243>
- Galusha, T., & Blick, J. C. (1971). Stratigraphy of the Santa Fe Group, New Mexico. *Bulletin of the American Museum of Natural History*, 144, 1–128.
- Gent, P. R., Yeager, S. G., Neale, R. B., Levis, S., & Bailey, D. A. (2010). Improvements in a half degree atmosphere/land version of the CCSM. *Climate Dynamics*, 34(6), 819–833. <https://doi.org/10.1007/s00382-009-0614-8>
- Grodsky, S. A., Carton, J. A., Nigam, S., & Okumura, Y. M. (2012). Tropical Atlantic biases in CCSM4. *Journal of Climate*, 25(11), 3684–3701. <https://doi.org/10.1175/jcli-d-11-00315.1>
- Hager, M. W. (1974). *Late Pliocene and Pleistocene history of the Donnelly Ranch vertebrate site, southeastern Colorado* (Vol. 2, p. 62). University of Wyoming. Contributions to Geology, Special Paper.
- Halliwell, G. R., Jr, & Allen, J. S. (1987). The large-scale coastal wind field along the west coast of North America, 1981–1982. *Journal of Geophysical Research: Oceans*, 92(C2), 1861–1884. <https://doi.org/10.1029/jc092ic02p01861>
- Hay, R. L., Pexton, R. E., Teague, T. T., & Kurtis Kyser, T. (1986). Spring-related carbonate rocks, Mg clays, and associated minerals in Pliocene deposits of the Amargosa Desert, Nevada and California. *Geological Society of America Bulletin*, 97(12), 1488–1503. [https://doi.org/10.1130/0016-7606\(1986\)97<1488:scrmca>2.0.co;2](https://doi.org/10.1130/0016-7606(1986)97<1488:scrmca>2.0.co;2)
- Haywood, A. M., Dowsett, H. J., Otto-Bliesner, B., Chandler, M. A., Dolan, A. M., Hill, D. J., et al. (2010). Pliocene model intercomparison project (PlioMIP): Experimental design and boundary conditions (Experiment 1). *Geoscientific Model Development*, 3(1), 227–242. <https://doi.org/10.5194/gmd-3-227-2010>
- Haywood, A. M., Tindall, J. C., Dowsett, H. J., Dolan, A. M., Foley, K. M., Hunter, S. J., et al. (2020). The Pliocene Model Intercomparison Project Phase 2: Large-scale climate features and climate sensitivity. *Climate of the Past*, 16(6), 2095–2123. <https://doi.org/10.5194/cp-16-2095-2020>
- Herbert, T. D., Lawrence, K. T., Tzanova, A., Peterson, L. C., Caballero-Gill, R., & Kelly, C. S. (2016). Late Miocene global cooling and the rise of modern ecosystems. *Nature Geoscience*, 9(11), 843–847. <https://doi.org/10.1038/ngeo2813>
- Hersbach, H., Bell, B., Berrisford, P., Hirahara, S., Horányi, A., Muñoz-Sabater, J., et al. (2020). The ERA5 global reanalysis. *Quarterly Journal of the Royal Meteorological Society*, 146(730), 1999–2049. <https://doi.org/10.1002/qj.3803>
- Hodges, K. I. (1996). Spherical nonparametric estimators applied to the UGAMP model integration for AMIP. *Monthly Weather Review*, 124(12), 2914–2932. [https://doi.org/10.1175/1520-0493\(1996\)124<2914:sneatt>2.0.co;2](https://doi.org/10.1175/1520-0493(1996)124<2914:sneatt>2.0.co;2)
- Hurrell, J. W., Hack, J. J., Shea, D., Caron, J. M., & Rosinski, J. (2008). A new sea surface temperature and sea ice boundary data set for the Community Atmosphere Model. *Journal of Climate*, 21(19), 5145–5153. <https://doi.org/10.1175/2008jcli2292.1>
- Ibarra, D. E., Oster, J. L., Winnick, M. J., Caves Rugenstein, J. K., Byrne, M. P., & Chamberlain, C. P. (2018). Warm and cold wet states in the western United States during the Pliocene-Pleistocene. *Geology*, 46(4), 355–358. <https://doi.org/10.1130/g39962.1>
- Knott, J. R., Machette, M. N., Klinger, R. E., Sarna-Wojcicki, A. M., Liddicoat, J. C., Tinsley, J. C., III, et al. (2008). *Reconstructing late Pliocene to middle Pleistocene Death Valley lakes and river systems as a test of pupfish (Cyprinodontidae) dispersal hypotheses. Late Cenozoic drainage history of the southwestern Great Basin and lower Colorado River region: Geologic and biotic perspectives* (Vol. 439, p. 1). [https://doi.org/10.1130/2008.2439\(01\)](https://doi.org/10.1130/2008.2439(01))
- Knott, J. R., Machette, M. N., Wan, E., Klinger, R. E., Liddicoat, J. C., Sarna-Wojcicki, A. M., & Weamer, V. M. (2018). Late Neogene-Quaternary tephrochronology, stratigraphy, and paleoclimate of Death Valley, California, USA. *Geological Society of America Bulletin*, 130(7–8), 1231–1255. <https://doi.org/10.1130/b31690.1>
- Kowalewska, A., & Cohen, A. S. (1998). Reconstruction of paleoenvironments of the Great Salt Lake Basin during the late Cenozoic. *Journal of Paleolimnology*, 20(4), 381–407. <https://doi.org/10.1023/a:1008053505320>
- Kurian, J., Li, P., Chang, P., Patricola, C. M., & Small, J. (2021). Impact of the Benguela coastal low-level jet on the southeast tropical Atlantic SST bias in a regional ocean model. *Climate Dynamics*, 56, 2773–2800. <https://doi.org/10.1007/s00382-020-05616-5>
- LaRiviere, J. P., Ravelo, A. C., Crimmins, A., Dekens, P. S., Ford, H. L., Lyle, M., & Wara, M. W. (2012). Late Miocene decoupling of oceanic warmth and atmospheric carbon dioxide forcing. *Nature*, 486(7401), 97–100. <https://doi.org/10.1038/nature11200>
- Lawrence, K. T., Liu, Z., & Herbert, T. D. (2006). Evolution of the eastern tropical Pacific through Plio-Pleistocene glaciation. *Science*, 312(5770), 79–83. <https://doi.org/10.1126/science.1120395>
- Lawrence, D. M., Oleson, K. W., Flanner, M. G., Thornton, P. E., Swenson, S. C., Lawrence, P. J., & Slater, A. G. (2011). Parameterization improvements and functional and structural advances in version 4 of the Community Land Model. *Journal of Advances in Modeling Earth Systems*, 3(1). <https://doi.org/10.1029/2011ms00045>

- Leduc, G., Garbe-Schönberg, D., Regenberg, M., Contoux, C., Etourneau, J., & Schneider, R. (2014). The late Pliocene Benguela upwelling status revisited by means of multiple temperature proxies. *Geochemistry, Geophysics, Geosystems*, 15(2), 475–491. <https://doi.org/10.1002/2013gc004940>
- Leopold, E. B., & Wright, V. C. (1985). Pollen profiles of the Plio-Pleistocene transition in the Snake River plain, Idaho. In C. J. Smiley (Ed.), *Late Cenozoic History of the Pacific Northwest* (pp. 323–348). American Academy of Sciences.
- Li, Z., Luo, Y., Arnold, N., & Tziperman, E. (2019). Reductions in strong upwelling-favorable wind events in the Pliocene. *Paleoceanography and Paleoclimatology*, 34(12), 1931–1944. <https://doi.org/10.1029/2019pa003760>
- Machette, M. N., Thompson, R. A., Marchetti, D. W., & Smith, R. S. (2013). Evolution of ancient Lake Alamosa and integration of the Rio Grande during the Pliocene and Pleistocene. *Geological Society of America Special Papers*, 494, 1–20. [https://doi.org/10.1130/2013.2494\(01\)](https://doi.org/10.1130/2013.2494(01))
- Mantua, N. J., & Hare, S. R. (2002). The Pacific decadal oscillation. *Journal of Oceanography*, 58(1), 35–44. <https://doi.org/10.1023/a:1015820616384>
- McClymont, E. L., Ford, H. L., Ho, S. L., Tindall, J. C., Haywood, A. M., Alonso-Garcia, M., et al. (2020). Lessons from a high-CO<sub>2</sub> world: An ocean view from ~3 Myr ago. *Climate of the Past*, 16(4), 1599–1615. <https://doi.org/10.5194/cp-16-1599-2020>
- Miller, M. D., & Tziperman, E. (2017). The effect of changes in surface winds and ocean stratification on coastal upwelling and sea surface temperatures in the Pliocene. *Paleoceanography*, 32(4), 371–383. <https://doi.org/10.1002/2016pa002996>
- Minnich, R. A. (2007). Climate, Paleoclimate, and Paleovegetation. In *Terrestrial vegetation of California* (3rd ed., pp. 43–70). University of California Press. <https://doi.org/10.1525/california/9780520249554.003.0002>
- Molnar, P., & Cane, M. A. (2002). El Niño's tropical climate and teleconnections as a blueprint for pre-Ice Age climates. *Paleoceanography*, 17, 1–11. <https://doi.org/10.1029/2001pa000663>
- Molnar, P., & Cane, M. A. (2007). Early Pliocene (pre-Ice Age) El Niño-like global climate: Which El Niño? *Geosphere*, 3(5), 337–365. <https://doi.org/10.1130/ges00103.1>
- Neale, R. B., Chen, C.-C., Gettelman, A., Lauritzen, P. H., Park, S., Williamson, D. L., et al. (2012). Description of the NCAR community atmosphere model (CAM 5.0). *NCAR Tech. Note NCAR/TN-486+STR*.
- O'Brien, C. L., Foster, G. L., Martínez-Botí, M. A., Abell, R., Rae, J. W., & Pancost, R. D. (2014). High sea surface temperatures in tropical warm pools during the Pliocene. *Nature Geoscience*, 7(8), 606–611.
- Philander, S. G., & Fedorov, A. V. (2003). Role of tropics in changing the response to Milankovitch forcing some three million years ago. *Paleoceanography*, 18(2). <https://doi.org/10.1029/2002pa000837>
- Pound, M. J., Tindall, J., Pickering, S. J., Haywood, A. M., Dowsett, H. J., & Salzmann, U. (2014). Late Pliocene lakes and soils: A global data set for the analysis of climate feedbacks in a warmer world. *Climate of the Past*, 10(1), 167–180. <https://doi.org/10.5194/cp-10-167-2014>
- Ravelo, A. C., Andreasen, D. H., Lyle, M., Lyle, A. O., & Wara, M. W. (2004). Regional climate shifts caused by gradual global cooling in the Pliocene epoch. *Nature*, 429(6989), 263–267. <https://doi.org/10.1038/nature02567>
- Ravelo, A. C., Dekens, P. S., McCarthy, M. (2006). Evidence for El Niño-like conditions during the Pliocene. *GSA Today*, 16(3), 4. [https://doi.org/10.1130/1052-5173\(2006\)016<4:efenlc>2.0.co;2](https://doi.org/10.1130/1052-5173(2006)016<4:efenlc>2.0.co;2)
- Reheis, M. C., Sarna-Wojcicki, A. M., Reynolds, R. L., Repenning, C. A., & Mifflin, M. D. (2002). In R. Hershler, D. B. Madsen, & D. R. Curry (Eds.), *Pliocene to middle Pleistocene lakes in the western Great Basin: Ages and connections. Great Basin aquatic systems history, Smithsonian Contributions to the Earth Sciences* (Vol. 33, pp. 53–108).
- Remeika, P., Fischbein, I. W., & Fischbein, S. A. (1988). Lower Pliocene petrified wood from the Palm Spring Formation, Anza Borrego Desert State Park, California. *Review of Paleobotany and Palynology*, 56(3–4), 183–198. [https://doi.org/10.1016/0034-6667\(88\)90057-7](https://doi.org/10.1016/0034-6667(88)90057-7)
- Salzmann, U., Haywood, A., Lunt, D., Valdes, P., & Hill, D. (2008). A new global biome reconstruction and data-model comparison for the middle Pliocene. *Global Ecology and Biogeography*, 17(3), 432–447. <https://doi.org/10.1111/j.1466-8238.2008.00381.x>
- Seager, R., Ting, M. F., Held, I., Kushnir, Y., Lu, J., Vecchi, G., et al. (2007). Model projections of an imminent transition to a more arid climate in southwestern North America. *Science*, 316(5828), 1181–1184. <https://doi.org/10.1126/science.1139601>
- Seager, R., & Vecchi, G. A. (2010). Greenhouse warming and the 21st century hydroclimate of southwestern North America. *Proceedings of the National Academy of Sciences*, 107(50), 21277–21282. <https://doi.org/10.1073/pnas.0910856107>
- Searles, Z. (2008). Mid-Pliocene (3.4–2.9 Myr) climate: Testing the atmospheric response of Pliocene sea surface temperatures (SST) revised to match proxy observations. *SOARS Manuscripts*. <https://doi.org/10.5065/qjh3-pz79>
- Small, R. J., Curchitser, E., Hedstrom, K., Kauffman, B., & Large, W. G. (2015). The Benguela upwelling system: Quantifying the sensitivity to resolution and coastal wind representation in a global climate model. *Journal of Climate*, 28(23), 9409–9432. <https://doi.org/10.1175/jcli-d-15-0192.1>
- Smith, G. A. (1994). Climatic influences on continental deposition during late-stage filling of an extensional basin, southeastern Arizona. *Geological Society of America Bulletin*, 106(9), 1212–1228. [https://doi.org/10.1130/0016-7606\(1994\)106<1212:ciocdd>2.3.co;2](https://doi.org/10.1130/0016-7606(1994)106<1212:ciocdd>2.3.co;2)
- Smith, G. A., Wang, Y., Cerling, T. E., & Geissman, J. W. (1993). Comparison of a paleosol-carbonate isotope record to other records of Pliocene-early Pleistocene climate in the western United States. *Geology*, 21(8), 691–694. [https://doi.org/10.1130/0091-7613\(1993\)021<0691:coapci>2.3.co;2](https://doi.org/10.1130/0091-7613(1993)021<0691:coapci>2.3.co;2)
- Smith, G. I. (1984). Paleohydrologic regimes in the southwestern Great Basin, 0–3.2 Myr ago, compared with other long records of “global” climate. *Quaternary Research*, 22(1), 1–17. [https://doi.org/10.1016/0033-5894\(84\)90002-4](https://doi.org/10.1016/0033-5894(84)90002-4)
- Smith, G. R. (1987). Fish speciation in a western North American Pliocene rift lake. *PALAIOS*, 2(5), 436–445. <https://doi.org/10.2307/3514615>
- Smith, G. R., & Patterson, W. P. (1994). Mio-pliocene seasonality on the Snake River plain: Comparison of faunal and oxygen isotopic evidence. *Paleogeography, Paleoclimatology, Paleoecology*, 107(3–4), 291–302. [https://doi.org/10.1016/0031-0182\(94\)90101-5](https://doi.org/10.1016/0031-0182(94)90101-5)
- Spall, M. A., & Schneider, N. (2016). Coupled ocean-atmosphere offshore decay scale of cold SST signals along upwelling eastern boundaries. *Journal of Climate*, 29(23), 8317–8331. <https://doi.org/10.1175/jcli-d-16-0109.1>
- Spencer, J. E., Patchett, P. J., Pearthree, P. A., House, P. K., Sarna-Wojcicki, A. M., Wan, E., et al. (2013). Review and analysis of the age and origin of the Pliocene Bouse Formation, lower Colorado River Valley, southwestern USA. *Geosphere*, 9(3), 444–459. <https://doi.org/10.1130/ges00896.1>
- Stuart, C. J., & Willingham, D. L. (1984). Late Tertiary and Quaternary fluvial deposits in the Mesilla and Hueco Bolsons, El Paso area, Texas. *Sedimentary Geology*, 38(1–4), 1–20. [https://doi.org/10.1016/0037-0738\(84\)90072-1](https://doi.org/10.1016/0037-0738(84)90072-1)
- Thompson, R. S. (1991). Pliocene environments and climates in the western United States. *Quaternary Science Reviews*, 10(2–3), 115–132. [https://doi.org/10.1016/0277-3791\(91\)90013-k](https://doi.org/10.1016/0277-3791(91)90013-k)
- Thompson, R. S. (1996). Pliocene and early Pleistocene environments and climates of the western Snake River Plain, Idaho. *Marine Micropaleontology*, 27(1–4), 141–156. [https://doi.org/10.1016/0377-8398\(95\)00056-9](https://doi.org/10.1016/0377-8398(95)00056-9)
- Thompson, R. S., & Fleming, R. F. (1996). Middle Pliocene vegetation: Reconstructions, paleoclimatic inferences, and boundary conditions for climate modeling. *Marine Micropaleontology*, 27(1–4), 27–49. [https://doi.org/10.1016/0377-8398\(95\)00051-8](https://doi.org/10.1016/0377-8398(95)00051-8)

- Tierney, J. E., Haywood, A. M., Feng, R., Bhattacharya, T., & Otto-Bliesner, B. L. (2019). Pliocene warmth consistent with greenhouse gas forcing. *Geophysical Research Letters*, *46*(15), 9136–9144. <https://doi.org/10.1029/2019gl083802>
- Wara, M. W., Ravelo, A. C., & Delaney, M. L. (2005). Permanent El Niño-like conditions during the Pliocene warm period. *Science*, *309*(5735), 758–761. <https://doi.org/10.1126/science.1112596>
- Winnick, M. J., Welker, J. M., & Chamberlain, C. P. (2013). Stable isotopic evidence of El Niño-like atmospheric circulation in the Pliocene western United States. *Climate of the Past*, *9*(2). <https://doi.org/10.5194/cp-9-903-2013>
- Wolfe, J. (1990). Estimates of Pliocene precipitation and temperature based on multivariate analysis of leaf physiognomy. In L. B. Gosnell, & R. Z. Poore (Eds.), *Pliocene climates: Scenario for global warming* (Vol. 90–64). US Geological Survey Open-File Report.
- Wycech, J. B., Gill, E., Rajagopalan, B., Marchitto, T. M., Jr, & Molnar, P. H. (2020). Multiproxy reduced-dimension reconstruction of Pliocene equatorial Pacific sea surface temperatures. *Paleoceanography and Paleoclimatology*, *35*(1), e2019PA003685. <https://doi.org/10.1029/2019pa003685>
- Zhang, Y. G., Pagani, M., & Liu, Z. (2014). A 12 Myr temperature history of the tropical Pacific Ocean. *Science*, *344*(6179), 84–87. <https://doi.org/10.1126/science.1246172>